

Bathymetry and geological structures beneath the Ross Ice Shelf at the mouth of Whillans Ice Stream, West Antarctica, modeled from ground-based gravity measurements

Atsuhiro Muto,¹ Knut Christianson,² Huw J. Horgan,³ Sridhar Anandakrishnan,¹ and Richard B. Alley¹

Received 7 May 2013; revised 16 July 2013; accepted 30 July 2013; published 20 August 2013.

[1] New gravity data reveal important geologic controls on the location and behavior of the grounding zone of Whillans Ice Stream (WIS), West Antarctica. Grounding zones of ice sheets and contiguous ice shelves are important for understanding ice sheet dynamics, as key processes that influence the grounded ice and its discharge into the ocean occur in these regions. Here, we model the bathymetry and shallow geological structures beneath the Ross Ice Shelf in an embayment of the WIS grounding zone using gravity data collected on the ground, in conjunction with seismic and radar data. We find that the region of shallow ocean water (<~50 m) is extensive; oceanographic models suggest that grounding zones exhibiting thin ocean cavities with gently sloping ice-ocean interfaces are likely to be tidally well mixed, leading to slower basal melting than would occur in a thicker, stratified water column. Beneath the ocean water column, we model a fault and a sedimentary basin in a half-graben, filled with two layers of sediments. The total thickness of the sediment layer is 900 to 1250 m in the half-graben, and 600 to 800 m on the upthrown block, and the basement depth is no more than 2000 m. We observe that the upper, softer sediment is thinnest near the modern grounding line and may possibly pinch out near our grid, and that the modeled fault is roughly parallel to part the grounding. We therefore hypothesize that the WIS grounding line stabilized in its current location in part due to the subglacial geology.

Citation: Muto, A., K. Christianson, H. J. Horgan, S. Anandakrishnan, and R. B. Alley (2013), Bathymetry and geological structures beneath the Ross Ice Shelf at the mouth of Whillans Ice Stream, West Antarctica, modeled from ground-based gravity measurements, *J. Geophys. Res. Solid Earth*, 118, 4535–4546, doi:10.1002/jgrb.50315.

1. Introduction

[2] The West Antarctic Ice Sheet (WAIS) has been a focus of extensive research to assess its recent changes and project future behavior in the context of global climate change. This is because much of the grounded part of WAIS lies on an inward-sloping bed that extends many hundreds of meters below sea level [Fretwell *et al.*, 2013]. This configuration makes the WAIS potentially vulnerable to rapid ice discharge after the loss of buttressing ice shelves, which could lead to retreat of the ice sheet-ice shelf junction [e.g., Hughes, 1977; Schoof, 2007; Joughin and Alley, 2011].

Additional supporting information may be found in the online version of this article.

¹Department of Geosciences and Earth and Environmental Systems Institute, Pennsylvania State University, Pennsylvania, USA.

²Department of Physics, St. Olaf College, Northfield, Minnesota, USA.

³Antarctic Research Centre, Victoria University of Wellington, Wellington, New Zealand.

Corresponding author: A. Muto, Department of Geosciences and Earth and Environmental Systems Institute, Pennsylvania State University, Deike Building, University Park, PA 16802, USA. (aum34@psu.edu)

©2013. American Geophysical Union. All Rights Reserved.
2169-9313/13/10.1002/jgrb.50315

[3] The grounding zone, where an ice stream meets an ice shelf, is of particular interest in understanding the mass balance of a marine ice sheet, as key processes that influence the grounded ice and its discharge into the ocean occur there. The WAIS currently is losing mass, with the majority of the imbalance originating from the Amundsen Sea coast and some from basins draining into Ronne Ice Shelf [King *et al.*, 2012; Shepherd *et al.*, 2012]; Siple Coast ice streams are near balance or gaining mass slightly [King *et al.*, 2012]. Attention thus is focused on the Amundsen Sea grounding zones. However, extensive crevassing greatly complicates fieldwork there, whereas the much greater accessibility of the Siple Coast grounding zones allows more extensive process studies. Furthermore, rigorous studies of Siple Coast grounding zones are warranted in order to understand their potential responses to possible reduction in buttressing from the Ross Ice Shelf [Walker *et al.*, 2012].

[4] Sedimentation at grounding zones can contribute to stability. For example, Whillans Ice Stream (WIS; formerly Ice Stream B) transports sediment subglacially [Blankenship *et al.*, 1987; Alley *et al.*, 1987; Kamb, 2001] and in the basal ice [Christoffersen *et al.*, 2009], with deposition of a grounding-zone wedge (“till delta”) [Alley *et al.*, 1989; Anandakrishnan *et al.*, 2007] from the subglacial till where flotation begins, and from englacial material where the base

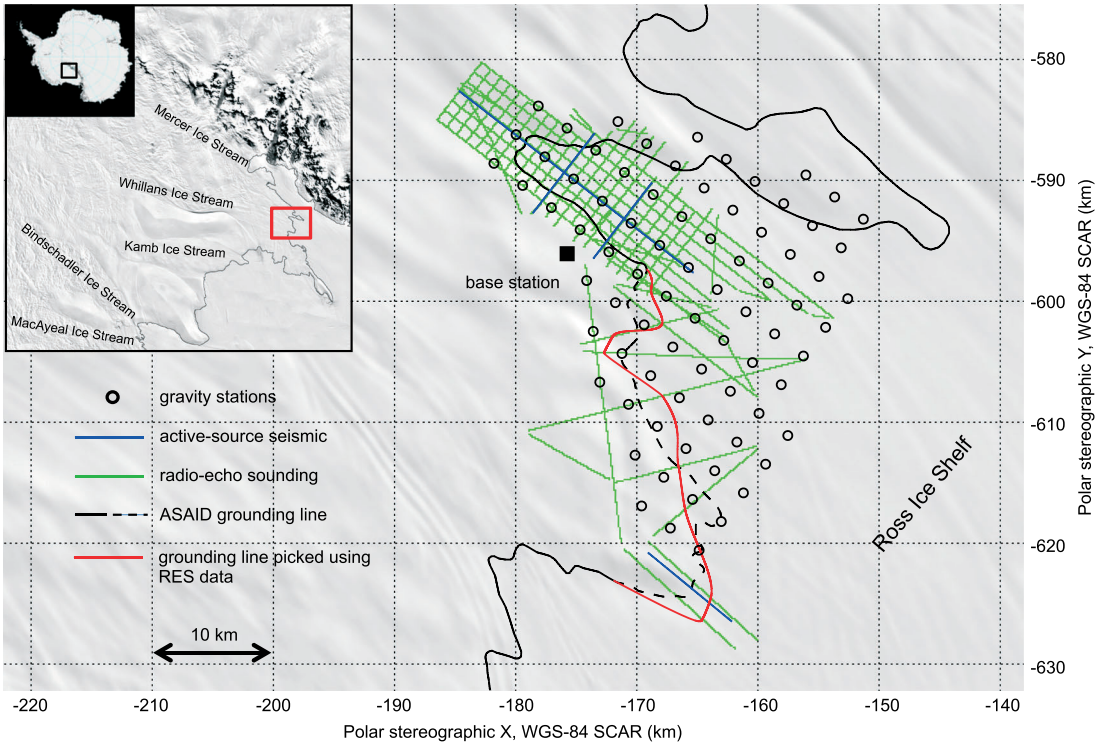


Figure 1. Map of the study area. Image is from MODIS MOA (MODIS Mosaic of Antarctica) [Haran et al., 2006]. Solid red line indicates the part of the grounding line picked by RES data (see text).

of the ice shelf melts. The ice-thickness increase caused by such a sediment wedge provides stability against grounding-zone retreat [Alley et al., 2007]. Such deposition is widespread around ice sheets, as shown by paleo records [e.g., Mosola and Anderson, 2006; Dowdeswell and Fugelli, 2012]. Thus, further knowledge of subglacial and submarine geological structures and their distributions contributes to understanding the present behavior and dynamic history of the glaciers and ice streams feeding the ice shelves [e.g., Anandakrishnan et al., 1998; Blankenship et al., 2001].

[5] The stabilizing role of sedimentation from melt-out of debris in ice highlights the importance of sub-ice-shelf melting [Christoffersen et al., 2009], which in turn is controlled in part by the water-column thickness and thus the history of sedimentation. In a sufficiently thick sub-ice-shelf water column, the ocean is generally stratified and a thermohaline circulation is established that maximizes the sub-ice-shelf melting near the grounding zone, whether the ocean water is cold or warm relative to the in situ ice melting point [e.g., Jenkins and Doake, 1991; Holland, 2008]. On the other hand, a thin water column (no more than several tens of meters) is tidally mixed, producing slower melting than in a stratified ocean, and tending to insulate the grounding zone from offshore ocean waters that could drive faster melting [Holland, 2008]. The bathymetry and the configuration of the cavity beneath ice shelves thus are key parameters influencing such ice-ocean interactions near the grounding zone. However, these characteristics are relatively poorly known for most Antarctic ice shelves.

[6] During the austral summer of 2011–2012, a comprehensive geophysical survey of the grounding zone was conducted as part of the Whillans Ice Stream Subglacial Access Research Drilling (WISSARD) Program [Fricker

et al., 2010]. Here, we report ground-based gravity observations and use these to estimate the water-column thickness and shallow (<3000 m deep) subglacial geology across the grounding zone. We use a three-dimensional gravity inversion technique constrained with radio echo sounding (RES) (Christianson et al., *Ice sheet grounding zone stabilization due to till compaction*, submitted to *Geophysical Research Letters*, 2013) and active-source seismology [Horgan et al., 2013]. Our gravity survey design allows a greater coverage than possible with the available seismic data (Figure 1), albeit with lesser spatial resolution.

2. Study Area

[7] We surveyed an area approximately 500 km² (Figure 1) centered on an embayment of the grounding zone where subglacial water is hypothesized to drain to the ice shelf [Carter and Fricker, 2012]. Ice thickness averages approximately 760 m on the grounded part, thinning to approximately 740 m at the seaward end of the survey (Christianson et al., *submitted to Geophysical Research Letters*, 2013). The ice velocity is approximately 340 m/yr [Rignot et al., 2011a]. In its lower reaches, Whillans Ice Stream moves rapidly during short diurnal or semidiurnal intervals interspersed with periods of little to no motion [Bindschadler et al., 2003].

[8] The water column beneath the ice shelf is generally thin near our study area. An extensive geophysical survey with gravity, active-source seismic and radar techniques was conducted during the Ross Ice Shelf Geophysical and Glaciological Survey (RIGGS) over four austral summers between 1973–1974 and 1977–1978, covering the entire Ross Ice Shelf and parts of the Siple Coast with an approximately 55 km grid. The water-column thicknesses at the RIGGS

stations G8 and G9, both situated approximately 30 km downstream of our study area, were 90 and 89 m, respectively, derived from the seismic data [Robertson and Bentley, 1990]. The water column thickens only gradually to 150 m in the next 200 km downstream of WIS [Albert and Bentley, 1990].

[9] Numerous studies [e.g., Bentley, 1987; Cooper *et al.*, 1991; Greischar *et al.*, 1992] have suggested that the Ross embayment, a large part of which is presently covered by the Ross Ice Shelf, accommodated major crustal extension between East and West Antarctica. Two distinct periods of extension have been identified: first during the late Mesozoic, with widespread graben formation and crustal thinning allowing sediment infilling, followed by more localized late Cenozoic deformation, mainly along the Transantarctic Mountains, Terror Rift, and Marie Byrd Land [Behrendt *et al.*, 1991; Cooper *et al.*, 1991; Karner *et al.*, 2005; Huerta and Harry, 2007; van Wijk *et al.*, 2008].

[10] Available data indicate that this general crustal structure extends beneath the Ross Ice Shelf and to the inner Ross Embayment. The dominant features mapped by the 55 km grid gravity data of RIGGS, as well as small-scale local gravity surveys at several locations with 10 to 20 km profiles [Grieschar *et al.*, 1992], were long-wavelength (>100 km) gravity anomalies paralleling the Transantarctic Mountains. Grieschar *et al.* [1992] suggested that the negative anomalies in both free-air gravity and Airy isostatic anomaly maps that cover parts of the Siple Coast, including our survey area (note that RIGGS gravity survey extended up to 150 km inland from the grounding zones in WIS and Kamb Ice Stream (KIS) regions), likely arise from thick glacial-marine sediments. A sediment-filled graben approximately 2500 m deep and 20 km wide has also been imaged by a combined seismic-refraction and gravity survey near Ridge BC between WIS and KIS, approximately 250 km inland of the current grounding line [Munson and Bentley, 1992]. We note that positive free-air and Bouguer gravity anomalies were observed for sedimentary basins and negative anomalies over basement highs in a large part of the Ross Sea north of the ice shelf; this “reversal” likely was caused by a delay in sedimentary basin filling, during which the lithosphere cooled and strengthened [Karner *et al.*, 2005; Bell *et al.*, 2006]. However, sedimentary basins of the inner Ross Embayment are relatively narrow (10–40 km wide) with sediment thicknesses of 1000–2500 m [Bell *et al.*, 2006]. Such narrow basins are likely analogous to the Terror Rift in the Ross Sea, which did not accommodate the same process as the wider Ross Sea due to its narrow width [Karner *et al.*, 2005].

3. Gravity Data

3.1. Data Acquisition and Processing

[11] Gravity measurements were made with a Scintrex CG-5 Autograv digital relative gravimeter (hereinafter “CG-5”). The CG-5 measures the relative differences in gravitational attraction by balancing the elongation of a fused-quartz proof mass by a spring and an electrostatic restoring force, where the restoring force is equal to the relative gravity value [Scintrex Limited, 2012; Koth and Long, 2012]. Most of the time, the CG-5 operated on two rechargeable internal 12 V lithium batteries. External 12 V lead-acid batteries (two

35 Ah or one 100 Ah) were connected to the CG-5 for storage and during long survey periods. The CG-5 was transported in a backpack carried by a surveyor traveling on a snowmobile. Special care was taken while in transit by traveling at less than 25 km/h and standing up to dampen jolts when driving on an uneven snow surface.

[12] Surveying was conducted on 8 separate days between 17 December 2011 and 5 January 2012. We made relative gravity measurements at 80 field stations (Figure 1), 64 of which were visited once, and 16 of which were visited two to four times, to provide multiple observations at survey crossover points. At each station, we averaged 2400 individual relative gravity observations, which were recorded at a 6 Hz sampling rate, after a settling period of approximately 3 min. To minimize tilting of the CG-5 from compression or melting of snow during the measurement, two pieces of wood (approximately $2.5 \times 5 \times 30$ cm) were first pressed into the snow surface. Then, a tripod and the CG-5 were placed on the wood pieces. CG-5 has an internal function to correct for tilt up to 200 arc seconds both in x - and y -planes [Scintrex Limited, 2012]. Tilt averaged approximately 10 arc seconds from level and never exceeded 50 arc seconds. We conducted the gravity survey under relatively calm conditions (<5 knots), but also utilized a wind block. An accurate position (horizontal and altitude) of each gravity station was determined from dual-frequency GPS data.

[13] To calculate the long-term instrument drift of CG-5, we established a local base station on grounded ice (Figure 1). Base-station measurements were made at the start and end of each day’s survey, and for >6 h at the start and end of the field season; these data were processed in the same way as the field-station measurements (relative gravity at the base station is shown in Fig. S1 of supporting information). Instrument drift was determined by fitting a fifth-order polynomial to all base-station measurements, following manufacturer recommendations [Scintrex Limited, 2012]. This drift correction accounts for residual nonlinear instrument drift induced by temperature variations in the gravimeter, voltage fluctuations, spring hysteresis, atmospheric pressure changes, and instrument transport [Torge, 1989; Koth and Long, 2012]. We did not observe any gravity signals at any station related to the horizontal movement due to the stick-slip motion of WIS [Bindschadler *et al.*, 2003].

[14] To tie the survey to absolute gravity, we made relative gravity measurements at the THIEL-1 gravity station at McMurdo Station [Wilson and Tinto, 2009] for 38 h before and 20 h after the field campaign. Absolute gravity measured at THIEL-1 in December 2011 as part of the POLENET program is 982970.200 mGal [Yves Rogister, personal communication, 2012].

[15] After drift correction, relative gravity observations were corrected for earth tide using the method of Longman [1959] and then converted to absolute gravity using the readings at THIEL-1. Finally, free-air gravity anomalies were calculated by applying the latitude and free-air corrections [Turcotte and Schubert, 2002]. For the 16 repeat occupation stations, an average free-air gravity anomaly was calculated and used in subsequent analysis. The uncertainty of individual free-air gravity anomalies at each station ranges from 0.022 to 0.059 mgal, with a mean of 0.032 mgal (supporting information). The root mean square (RMS) of crossover differences, which is a common measure of uncertainty in gravity

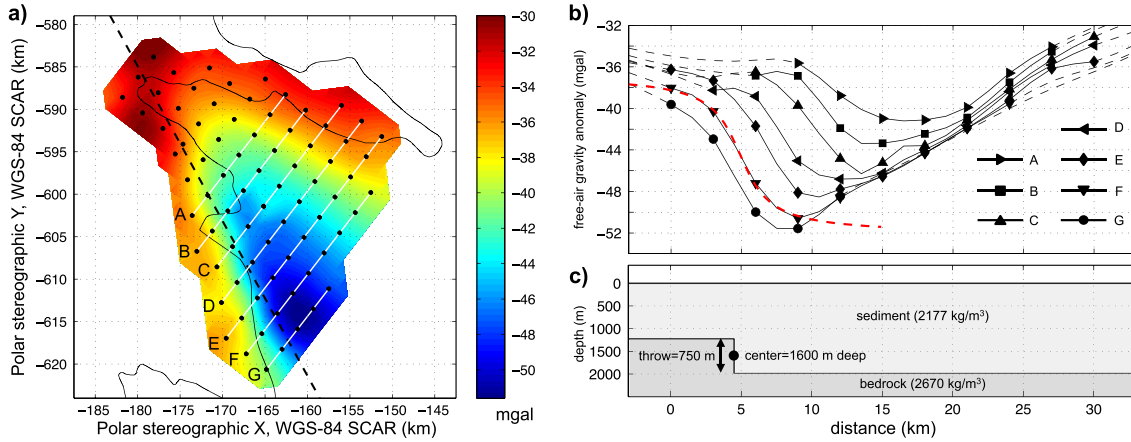


Figure 2. (a) Free-air gravity anomaly map of the study area. Black dots are gravity stations. White lines and capital letters correspond to profiles shown in Figure 2b and thick dashed line is the estimated direction the fault. (b) Two-dimensional profiles of free-air gravity anomalies along white lines in Figure 2a. Dashed lines indicate extrapolated values. Red dashed line is a profile simulated with vertical fault with a throw (h) of 750 m with its center at a depth (z_0) of 1600 m. (c) Schematic of the fault model used to simulate the gravity anomaly profile indicated by the thick dash-dot line in Figure 2b.

surveying [e.g., *Wessel and Watts*, 1988], was 0.111 mGal at repeat occupation stations. Our RMS crossover difference of 0.111 mgal is approximately four times larger than our calculated single-observation uncertainty of the free-air anomaly. There could be several factors contributing to this relatively large RMS crossover difference compared to the uncertainty of individual free-air anomalies. Tares in the spring could have occurred despite the precautions taken in handling the CG-5, and other environmental factors resulting in instrument drift could also be contributing. However, the RMS crossover differences are small when compared to the calculated gravity anomalies. We use the RMS crossover difference as the overall uncertainty of the free-air gravity anomalies in the inversion.

[16] We note that there are inconsistencies in the use of the term “gravity anomaly” in geodesy and geophysics [*Hackney and Featherstone*, 2003]. We applied the free-air correction using the reference acceleration of gravity defined by the 1980 Geodetic Reference System (GRS 80) Formula [*Turcotte and Schubert*, 2002], which uses the ellipsoid as the reference surface; hence, the “free-air gravity anomaly” we computed here is the “gravity disturbance” as defined in geodesy [*Hackney and Featherstone*, 2003]. However, we use the term “free-air gravity anomaly” throughout the text, following previous geophysical investigations using gravity anomalies in Antarctica [e.g., *Greischar et al.*, 1992; *Diehl et al.*, 2008].

3.2. Free-Air Gravity Anomaly Map

[17] Free-air gravity anomalies range from -51.5 to -30.1 mgal, with a general pattern of lower anomalies over the floating ice. For subsequent analysis, free-air gravity anomalies were gridded and interpolated (extrapolated beyond the area of the survey) to a 1.5 by 1.5 km grid (Figure 2a) using the biharmonic spline interpolation [e.g., *Sandwell*, 1987].

[18] Steep gradients in the gravity anomaly run through the grid-western half of the survey area, trending grid north-northwest to south-southeast. Two-dimensional profiles in Figure 2b indicate that the steepest gradient is 2.3 mgal/km

between coordinates $(-166\text{ km}, -616\text{ km})$ and $(-164\text{ km}, -614\text{ km})$, ~ 3 km offshore of the grounding line.

4. Supporting Data

[19] Data collected by active-source seismic and radio echo sounding (RES) surveys were used as constraints in the interpretation of the gravity data. Active-source seismic data were collected along the lines shown in solid blue in Figure 1 [*Horgan et al.*, 2013]. We constrain our gravity inversion using the seismically imaged thicknesses of the water column and upper sediment layer (see next section for descriptions). Low-frequency (5 MHz) RES data (*Christianson et al.*, submitted to *Geophysical Research Letters*, 2013) provided regional constraints on the ice thickness (green lines, Figure 1). In addition to the surface elevation data collected with a GPS unit during the gravity survey, we used the GPS data collected along RES profiles to map surface elevation over the survey area. Detailed descriptions on active-source seismic and RES surveys can be found in *Horgan et al.* [2012; 2013] and *Christianson et al.* [2012; submitted to *Geophysical Research Letters*, 2013], respectively. Surface elevation and ice thickness were gridded using the same method as for the free-air gravity anomaly.

[20] All data will be made available digitally through the Antarctic Glaciological Data Center at the National Snow and Ice Data Center (<http://nsidc.org/agdc/>) in the near future.

5. Gravity Inversion

5.1. General Model

[21] We model our study area as a layer of snow and ice overlying a water column, sedimentary layer, and basement rock. This approach is consistent with inversion of subglacial structures in various parts of Antarctica [e.g., *Greischar et al.*, 1992; *Studinger et al.*, 2004; *Muto et al.*, 2013].

[22] The negative free-air anomalies covering the study area (Figure 2a) suggests that it is underlain by sediments, consistent with results of the RIGGs gravity survey [*Greischar*

et al., 1992]. This interpretation is supported by the results of seismic surveys within a ~200 to 300 km radius of our study area [Robertson *et al.*, 1982; Rooney *et al.*, 1987; Robertson and Bentley, 1990] that imaged a sediment layer ~700 to 1500 m thick. Our relatively large negative free-air gravity anomalies, compared to other parts of the Greischar *et al.* [1992] survey, suggest that the survey area overlies a sediment-filled graben. The steep gradient on one side of our survey indicates that a fault with large offset may be present. We first discuss modeling the ice, water, and upper sediment layer, and then provide more details on treatment of the fault.

5.2. Bathymetry and Sedimentary Structure

[23] To invert the free-air gravity anomalies for bathymetry and sediment-layer thicknesses, we used the forward model of Plouff [1976]. Here, the domain of interest is discretized into small 3-D rectangular prisms, with three layers of different densities sitting on the basement rock (2670 kg/m^3), which is assumed to be a half-space. The upper layers comprise: ice (average density of $\rho = 890 \text{ kg/m}^3$), seawater where indicated ($\rho = 1030 \text{ kg/m}^3$), upper sediment layer (2014 kg/m^3 appropriate for rock of 40% porosity with voids filled with seawater), and lower sediment layer (2178 kg/m^3 , appropriate for rock of 30% porosity). Density contrasts of each of the three layers with the basement are used to calculate the gravity anomaly arising from each prism.

[24] To determine an appropriate ice density to use in our inversion, we first determined the density profile of the firn from shallow seismic-refraction velocities collected during seismic surveying, following the method of Kohnen and Bentley [1973]. We then extrapolated this density profile to the density of pure ice (917 kg/m^3) following the method of Severinghaus *et al.* [2010] and integrated the density profile for the entire firn/ice column. The density of seawater (1030 kg/m^3) is taken from Holland [2008].

[25] We based our two-layered sediment model on the active-source seismic results of Horgan *et al.* [2013]. For RIGGS sites within ~200 km radius of our study area, Robertson and Bentley [1990] imaged a seismic reflector 50–150 m beneath the sea bottom, similar to that observed in our study area by Horgan *et al.* [2013]. A long-refraction survey by Robertson and Bentley [1990] also showed the thickness of the whole sediment layer to be 500–2000 m. Those data do not preclude the possibility that the whole sediment layer consists of more than two layers of different densities. However, as we imaged one prominent subbottom reflector in our active-source seismic data, we chose to use a simple sediment-over-basement model. We did not include the thin till layer ($<= 19 \text{ m}$) imaged by active-source seismics. If we assume a soft, deforming till with the density of 1750 kg/m^3 [Peters *et al.*, 2007], which we consider to be the low end of the possible densities for till, a step change in the thickness of such a layer from 0 to 20 m buried ~750 m deep beneath ice causes a gravity anomaly of only 0.2 mgal, small compared to the overall RMS misfit of 0.6 mgal between the observed free-air gravity anomalies and those simulated by our preferred model, as described below. We therefore consider the inclusion of such a thin till layer unnecessary.

[26] Sediment density is not tightly constrained by available data. Seismic P wave velocities of the uppermost

sediment layer at nearby RIGGS sites were 2500–2600 m/s [Robertson and Bentley, 1990] (velocities of 1200 and 3200 m/s were also reported but those values were thought to be affected by the dip in the bed), which can be converted to around 2100 kg/m^3 using widely accepted empirical relation between seismic velocity and density [Nafe and Drake, 1963]. Rooney *et al.* [1991] reported velocities of 1900–2250 m/s for the sediment beneath WIS approximately 300 km upstream of our study area, corresponding to densities of ~ 1700 – 2250 kg/m^3 . Based on these data, and insights from other Antarctic gravity studies [Roy *et al.*, 2005; Muto *et al.*, 2013], we chose 2014 kg/m^3 (40% porosity) for the upper layer and 2178 kg/m^3 (30% porosity) for the lower layer.

[27] Seismic P wave velocity of the upper sediment layer was not separately measured, but is needed to derive the layer thickness from the two-way travel time obtained by the active-source seismic survey. We estimated seismic velocity (V_P) from the density (ρ), using the polynomial fit of Onizawa *et al.* [2002] to the data for sedimentary rocks of Nafe and Drake [1963],

$$V_P = 6.86 - 7.55\rho + 2.64\rho^2. \quad (1)$$

[28] With our estimated density of 2014 kg/m^3 , V_P is 2362 m/s .

[29] The observed and calculated gravity anomalies are offset by a constant shift [Jacoby and Smilde, 2009], often called DC shift [e.g., Tinto and Bell, 2011], because the method we used here calculates the absolute gravity anomaly whereas the free-air gravity data are in reference to the geoid. Also, the observed free-air gravity anomaly contains signals from large-scale geological structures such as the crustal thickness and the Moho structure [e.g., Studinger *et al.*, 2004] that create regional gravity anomalies on wavelengths longer than our survey area. We determined this DC shift by searching for a plane that minimizes the RMS difference between the observed and calculated gravity anomalies at 82 gravity stations. Our implementation of the DC shift is equivalent to combining two corrections that are usually treated separately: (1) correcting for the depth of the basement rock that is a part of a frequently used Parker-Oldenburg technique [Parker, 1973; Oldenburg, 1974]; (2) correcting for the regional trend in the free-air gravity anomaly [Studinger *et al.*, 2004; Filina *et al.*, 2008].

5.3. Fault Structure

[30] As noted above, there are steep gravity-anomaly gradients in our survey area, which suggests the presence of a fault. Greischar *et al.* [1992] showed from analysis of a 2-D gravity profile obtained near Roosevelt Island that gravity gradients of similar magnitude to ours can be produced by a vertical fault with a throw of 400 m, with its center buried at a depth of 1.3 km beneath sediments [Grieschar *et al.*, 1992, Figure 15]. Greischar *et al.* [1992] also noted that similar faults occur at several locations beneath the Ross Ice Shelf. These lines of evidence motivated us to model a vertical fault in the basement rock beneath our survey area. Since a vertical fault causes the steepest gradient in the gravity anomaly directly above the fault [e.g., Lowrie, 2007], we estimated the direction of

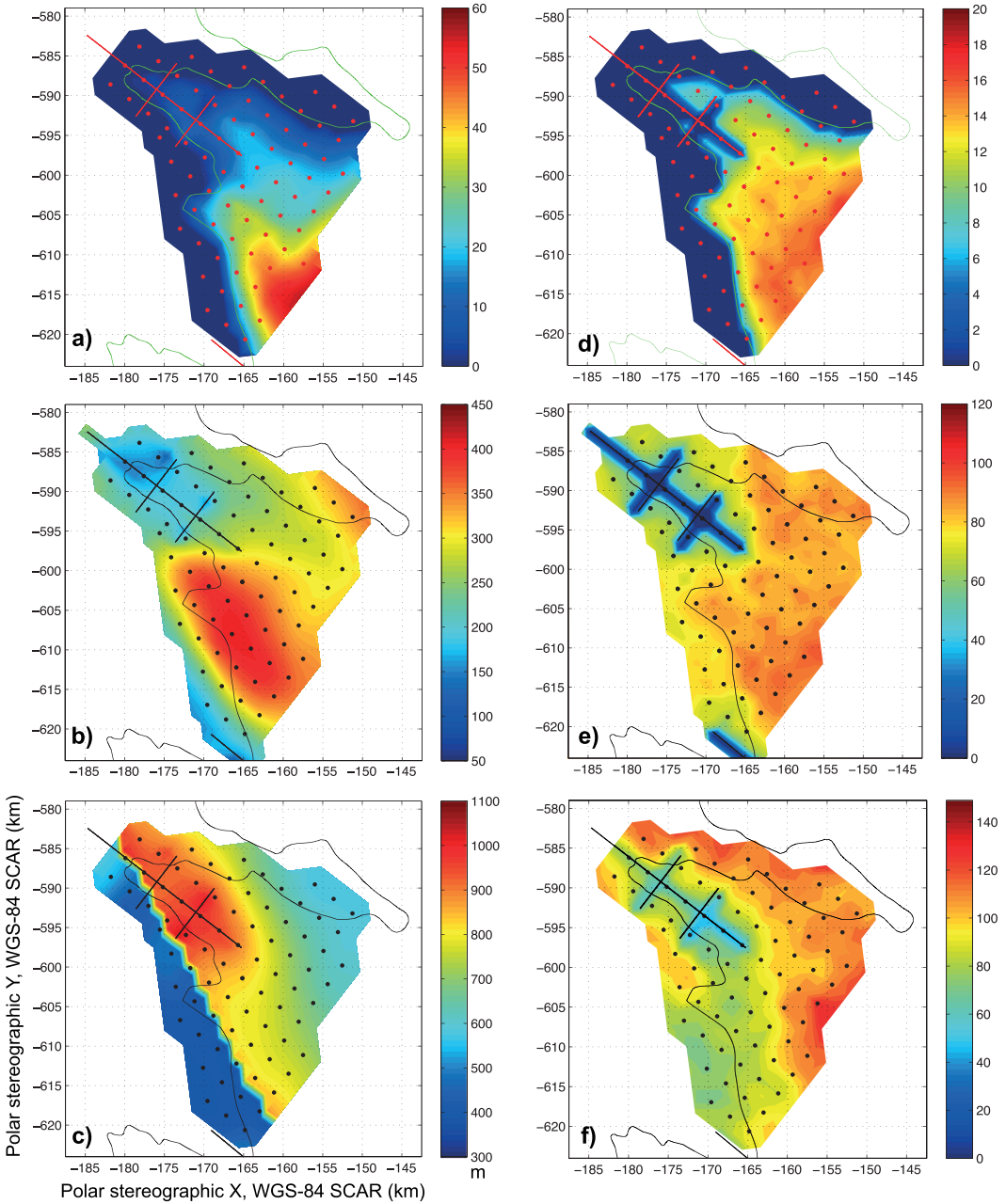


Figure 3. Models of thicknesses of (a) water column, (b) upper sediment layer, and (c) lower sediment layer, with their 2σ uncertainties in Figures 3d to 3f, respectively.

the fault by first finding the point of the steepest gradient along the seven 2-D profiles (white lines, Figure 2a), then calculating the best fit line through those seven points in the x - y grid space using the least squares method. The black dotted line in Figure 2a shows our estimate of the strike of the fault.

[31] Before carrying out the inversion, we obtained an estimate of the throw and the depth of the fault by comparing 2-D profiles of the gravity anomaly along the profile F, where the steepest gradient in the gravity anomaly was observed, with those calculated using the equation of Lowrie [2007] (equation (2)). Equation (2) approximates the gravity effect

of a vertical fault Δg_{vf} with a throw of h with the center at depth z_0 (Figure 2c);

$$\Delta g_{vf} = 2G\Delta\rho h \left[\frac{\pi}{2} + \tan^{-1} \left(\frac{x}{z_0} \right) \right], \quad (2)$$

where G is the universal gravitational constant ($6.67 \times 10^{-11} \text{ m}^3/\text{kg s}^2$), $\Delta\rho$ is the density contrast ($2670 - 2178 = -492 \text{ kg/m}^3$ in this case) and x is the horizontal distance from the fault (Figure 2c). We determined that a vertical fault with $h = 750 \text{ m}$ and $z_0 = 1600 \text{ m}$ (Figure 2c) gives a good approximation to the observed gravity anomaly (red dashed line

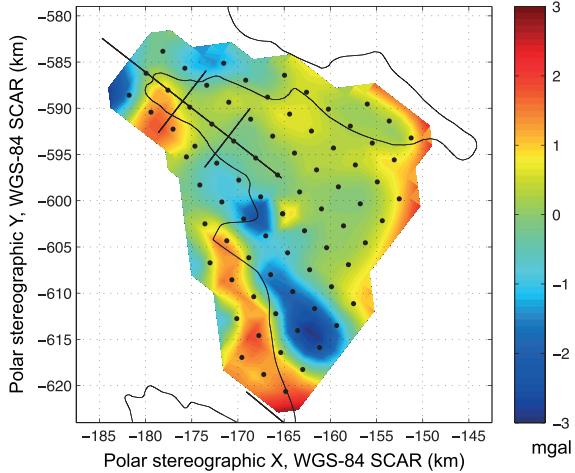


Figure 4. Misfit between observed and modeled free-air gravity anomalies.

in Figure 2b). This estimate assumes that the fault affects gravity solely by juxtaposing basement and the deeper sedimentary layer, but it is likely that the fault also juxtaposes lower-density and higher-density sedimentary layers that contribute to the anomaly, so the model probably overestimates the offset needed to explain the gravity anomaly.

Therefore, even including uncertainties, the full inversion should not require much more offset than given from application of equation (1), so we limited the depth of the interface between the basement and the lower sediment layer to 2000 m.

[32] We performed our full inversion using Very Fast Simulated Annealing (VFSA), which has been employed in modeling the bathymetry and the sediment-layer thickness of Lake Vostok [Roy *et al.*, 2005; Filina *et al.*, 2008] and beneath the ice shelf of Pine Island Glacier [Muto *et al.*, 2013]. The details of our implementation are presented in Muto *et al.* [2013], and not repeated here. We ran the VFSA algorithm repeatedly to generate 5000 models with different starting guesses and derived the posterior probability density distribution (PPD). The mean of the PPD is presented as our most likely model, and we report model uncertainties as the 95% confidence interval (approximately two standard deviations).

[33] To speed up the forward calculation, we included the gravity effect of only those prisms within a 25.5 km radius of a particular point. This radius was selected after several exploratory computations, as the contribution of the blocks beyond 25.5 km is less than the uncertainty in the free-air anomaly data. We further reduced the computational time for convergence to the optimal model by using a smoothing filter when perturbing the model, employing a 5:1 weighting of a prism with the eight nearest neighbors in a layer. To simulate the fault in the basement rock, we applied the smoothing filter to our estimated upthrown and downthrown blocks separately when perturbing the interface between the lower sediment layer and the basement.

[34] It is best to introduce as much a priori information as possible to constrain the gravity inversion, since it is an inherently nonunique problem [e.g., Jacoby and Smilde, 2009]. We used the grounding-line position from the Antarctic Surface Accumulation and Ice Discharge (ASAID) [Bindschadler *et al.*, 2011; solid black line in Figure 1], supplemented by the grounding-line position we picked from

RES data in some parts (solid red line in Figure 1). We favored ASAID over MEaSUREs (Making Earth Science Data Records for Use in Research Environments) [Rignot *et al.*, 2011b] because the MEaSUREs grounding line is discontinuous in our study area. In addition to remotely sensed grounding lines, we also identified the basal expression of grounding from RES data. In areas of active subglacial sedimentation, the grounding line is marked by irregular basal ringing in RES data that extends well below the ice-bed interface, which we interpret as reflections from on- and off-nadir seawater-saturated sediments that occur only in the vicinity of grounding. Where little or no active sedimentation is occurring, extensive basal crevassing frequently marks the grounding line. Furthermore, internal reflecting horizons often fold dramatically just upstream of grounding in response to increased basal friction due to compaction of subglacial till from repeated tidal flexure (Christianson *et al.*, submitted to *Geophysical Research Letters*, 2013). Together these metrics provide a relatively robust estimate of grounding line location. We note that basal reflectivity contrast is useful to indicate the length of the grounding zone, but is too indistinct and gradual to indicate the precise location of grounding. Thicknesses of ice, water column, and upper sediment layer were constrained with active-source seismic and RES data as already discussed in the previous section.

6. Inversion Results

[35] Figures 3a to 3c show models of the thicknesses of the ocean water column, and the two sediment layers obtained from our gravity inversion, with the 95% confidence intervals shown in Figures 3d to 3f. The fault appears pixelated in Figure 3c (and in Figure 5) because it runs at an angle of approximately 30° to the 1.5 by 1.5 km grid that we used. We report 2σ uncertainty values here, because we found that the majority of PPDs can be approximated with a Gaussian distribution. Misfits between the observed free-air gravity anomalies and those calculated from our inverted model are shown in Figure 4. The RMS misfit within the survey area is 0.595 mgal, and all misfits are within ± 2.40 mgal. Large misfits are restricted to near the edge of the survey area, for example around coordinates (-182 km, -588 km) and (-170 km, -617 km). These edge effects are caused by imperfect extrapolation of free-air anomalies beyond the survey area. However, most of these misfits decrease rapidly into the survey area, to less than ± 1 mgal within one or two grid cells (1.5 to 3 km); thus, the edge effects do not affect our interpretations, since we do not focus on small-scale features. Although the RMS misfit (0.595 mgal) is about six times larger than the uncertainty of the observed free-air anomaly, it is a reasonable value given the uncertainty in the inverted model. If, for example, we perturb the best fit model by shifting the thickness of the water column and the upper sediment layer to their lower uncertainty bounds (2σ), which makes them 12 and 70 m thinner on average, respectively, and make the lower sediment layer thicker accordingly, the RMS misfit increases to 1.30 mgal. Since perturbing the model within the uncertainty bounds doubles the RMS misfit, we consider that misfits obtained with the most likely model are satisfactory. We also recognize that our assumptions for densities of subsurface materials, and uniform

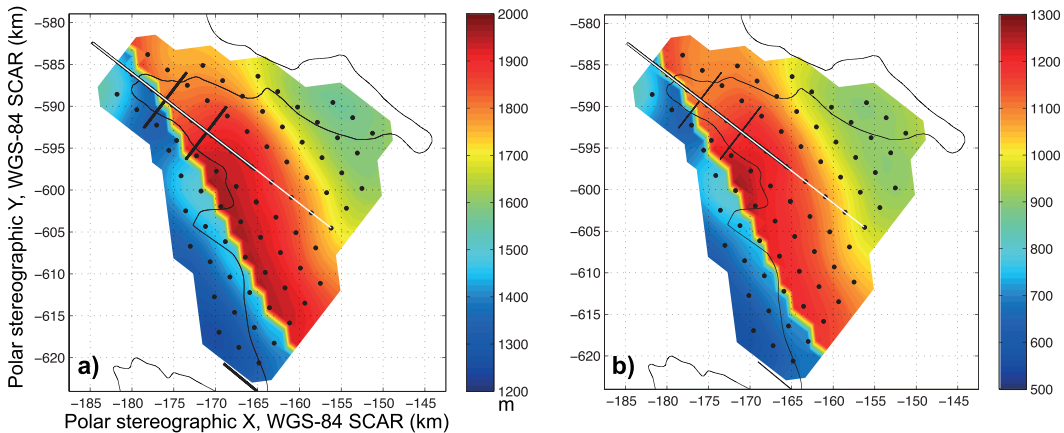


Figure 5. (a) Depth to the basement rock and (b) total thickness of sediment (upper + lower layers). White lines indicate the position of the cross section in Figure 6.

density within each layer, are unlikely to be exactly correct, with deviations probably contributing to the misfit.

6.1. Water Column

[36] The water column is generally thin in the embayment. The maximum water-column thickness is 52 ± 18 m, at the seaward edge of the study area near coordinate (-160 km, -615 km) (Figure 3a). The seismic survey revealed that the water column is less than 16 m thick within the narrow, landward-most part of the embayment (Figure 3a) (see also Horgan *et al.* [2013], for detailed discussions). Also, the maximum water-column thickness along one seismic-survey line situated just outside of our gravity survey grid was 15 ± 2 m at the seaward end of the line, approximately 5 km from the grounding line [Horgan *et al.*, 2013], generally consistent with our results.

[37] We note that it is possible that our inversion is slightly overestimating water-column thickness, and also the thickness of the upper sediment layer, moving away from the seismic lines used to constrain the model. This is suggested by the rapid increase in water-column thickness away from the seismic lines (red solid lines in Figure 3a), which could represent a true feature of the embayment, but also could represent the tendency of inversions such as this to concentrate structures near the surface where they can have the most influence on the gravity field [Li and Oldenburg, 1998]. However, the inversion allowed the water-column thickness to be as much as 300 m, and the maximum thickness returned was only 52 m. Thus, the water column is thin throughout the embayment (<50 m) and thickens away from the grounding zone beneath the ice shelf.

6.2. Sediment Column

[38] The thickness distribution of the upper sediment layer exhibits some similarities to the water column, increasing in thickness grid-southeastward from the grounding zone along flow beneath the Ross Ice Shelf, and increasing away from the seismic lines. Our best assessment based on experience with the inversion and the error structure is that the thickening is real but the magnitude may be overestimated, with the true thickness away from the seismic lines closer to the lower uncertainty bound. We note that we obtain a thin water column and upper sediment column thickening downstream

of the grounding zone if we conduct the inversion without specifying a fault (supporting information, Fig. S2); this is a robust result of the gravity data.

[39] The modeled basement topography suggests that the study area is centered over a half-graben, with the depth varying from 1500 to 1600 m at the grid northeastern edge of the study area to just under 2000 m at the fault (Figure 5a). The dip in this half-graben is approximately 1°, calculated between coordinates (-170 km, -602 km) and (-151 km, -593 km), in a direction approximately normal to the fault. The throw of the fault is ~450–500 m. The total thickness of the sediment layer (upper and lower sediment layers combined) varies from 900 to 1250 m in the half-graben, and 600 to 800 m on the upthrown block (Figure 5b). If the thicknesses of the water column and the upper sediment layer are overestimated, as suggested above, then a consistent solution would increase the fault throw and decrease the maximum depth of the half-graben and the total thickness of the sediment package.

7. Discussion

[40] Our results provide insights into the ocean cavity, subice-shelf sediment, and geologic structures, and controls on the grounding-line position (Figure 6).

[41] Many processes may affect ocean circulation and melting beneath ice shelves. The density-driven “ice pump” circulation [Lewis and Perkin, 1986] is especially important where the seafloor slopes downward toward a deep grounding line in a fairly thick water cavity, driving rapid melt. Tidal processes are also important for ice shelves [e.g., Williams *et al.*, 1998; Makinson *et al.*, 2012]. In shallow water and very near the grounding line, the ice pump circulation becomes ineffective and a well-mixed zone tends to develop across a tidal front, causing melting to be slower than in the density-driven flow [Holland, 2008]. The tidal front could be as close to the grounding line as 12.5 km for some parts of the Ross Ice Shelf where the slope of the water-column thickness is 0.1 % [Holland, 2008]. However, our results indicate that the slope of the water-column thickness is less than 0.01% everywhere in our study area; hence, the tidal front is most likely farther offshore than the limit of our study area. The extensive, thin water layer we estimate

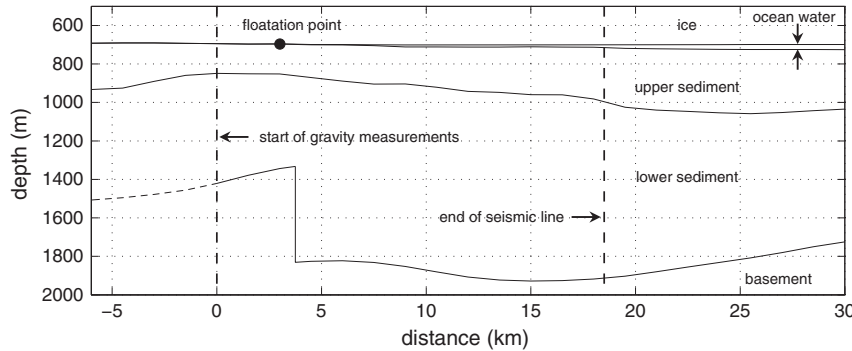


Figure 6. Cross section of the model along the white line in Figure 5. Floatation point is from *Horgan et al.* [2013], derived from seismic and GPS surveys.

for the embayment indicates that it is filled with tidally well-mixed ocean, driving slower melting and thus slower but more distributed sedimentation from dirty basal ice, than would otherwise occur [e.g., *Holland et al.*, 2003]. The additional bathymetric constraints provided by our results in this zone may aid in tide modeling [*Padman et al.*, 2003].

[42] The modern grounding line of the Siple Coast, especially WIS, is more convoluted than grounding lines in other regions of Antarctica, with flow essentially parallel to the grounding line in some places. Sedimentation may eventually fill embayments and create prograding sediment wedges resulting in a more uniform grounding zone [e.g., *Dowdeswell, et al.*, 2008]. However, the available paleo-data provide indirect indications that the WIS grounding line probably did not reach the vicinity of its current position until sometime in this millennium [*Hulbe and Fahnestock, 2004; Catania et al., 2012*]. Of particular relevance, thinning at Reedy Glacier flowing into Mercer Ice Stream (formerly Ice Stream A) and likely linked to grounding-line retreat continued from an ice-age maximum into the most recent millennium [*Todd et al., 2010*], consistent with other evidence indicating late-Holocene retreat of the grounding line of the Ross Ice Shelf [*Conway et al., 1999*]. Hence, the modern grounding-line position likely has not been greatly modified by recent sedimentation [also see *Catania et al., 2012*].

[43] The upper layer of lower density sediment is relatively thick beneath the ice shelf in the grounding-line embayment in our survey region. The grounding line is subparallel to the transition from thicker to thinner upper sediment layer beneath grounded ice, especially on the grid-western side of the embayment, across a fault as described below. The match is not perfect, and nowhere does our inversion return a zero-thickness upper sediment layer. However, considering the resolution of the data, and the possible contribution of a deforming till layer to the upper sediment layer, it remains possible that this less dense and softer sediment is locally absent. We thus hypothesize that the Holocene grounding-line retreat stabilized near its present position in part because of structurally controlled local topographic highs, followed by local sediment deposition resulting in stabilizing feedbacks such as those detailed in *Alley et al.* [2007].

[44] Inversions converge to a solution with thin water layer (<50 m) and thin upper layer sediments regardless of the presence of a fault in the starting model (Supplementary material Fig. S2). Moreover, the steep slope in the basement

rock that is produced by the inversion without specifying a fault could be interpreted as a fault at a steep angle (Supplementary material Fig. S4). However, the steep gravity gradient strongly suggests presence of a vertical or near-vertical fault, as does the general geologic setting (see below), and introducing the vertical fault reduces the misfit of the inversion (RMS misfit is 1.067 mgal without specifying the fault, almost twice as large as the 0.595 mgal with the fault). We note that the modeled fault falls very close to a segment of the grounding line that is nearly parallel to ice flow, with grounded ice on the upthrown side, further suggesting a geological control.

[45] We also note that Crary Ice Rise (CIR) occupies the upthrown side of a linear continuation of the fault. CIR is an elevated feature on the surface of grounded ice, rising nearly 50 m above the surrounding ice shelf [*Bindschadler, 1993*]. A seismic-refraction survey conducted on CIR [*Robertson et al., 1982*] found 750 m of sediment above basement beginning 1200 m below sea level, values that are close to our modeled values on the upthrown side of 600–800 m total sediment thickness and basement 1300–1500 m below sea level. We therefore speculate that the fault may continue at least that far and that the ice rise is controlled by the fault (Figure 7).

[46] As discussed in section 2, there is extensive evidence from north of the Ross Ice Shelf for persistent or repeated rifting of the Ross Embayment, including near the front of the Transantarctic Mountains, and for sedimentation in those rifts. The more limited data from beneath the Ross Ice Shelf and the Siple Coast Ice Streams suggest continuation of those trends, consistent with our results [e.g., *Rooney et al., 1987; Greischar et al., 1992*].

[47] The structure of the sediment layer and the basement rock we modeled here is generally similar to those found by *Grieschar et al. [1992]* from the local gravity survey at J9DC (Figure 7), which is one of the RIGGS sites closest to our survey area, situated approximately 200 km to grid south, and thus somewhat farther from the Transantarctic Mountains. There, *Grieschar et al. [1992]* found a steep gravity gradient, of 1.8 mgal/km, increasing from grid southwest to northeast, which is similar in magnitude and direction to the steep gradient that we modeled as a fault. They simulated this gravity profile with a vertical fault in the basement rock with the throw of 600 m, centered at 1500 m deep, with the grid southwestern part downthrown. They modeled a single sediment layer, of thickness 600–700 m on the upthrown side

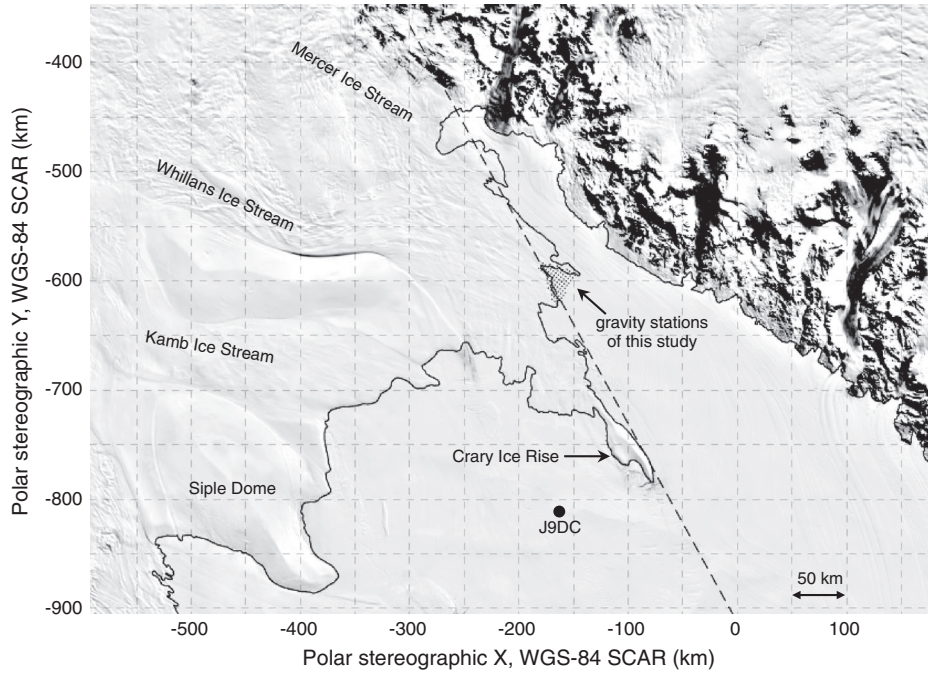


Figure 7. Map of a part of Siple Coast showing locations of Crary Ice Rise and the estimated orientation of the fault (black dashed line). The image is from MODIS MOA and the black solid line is the grounding line from ASAID.

and 1100–1200 m on the downthrown side; this was compatible with the results of the seismic-refraction survey of Robertson and Bentley [1990], who inferred sediment-layer thickness of ~1400 m [Greischar et al., 1992]. Our study area and J9DC are located 200 km apart and on opposite sides of the grounded ice plain that leads to CIR. One possible interpretation is that this topographically high region with relatively high gravity and thin sediments represents a horst, separated from grabens or half-grabens by the faults identified by Greischar et al. [1992] and in our study. Clearly, our limited gravity survey cannot test all of these hypotheses, but may serve to help guide further work.

8. Conclusions

[48] We used a high-resolution ground-based gravity data set to model the bathymetry and shallow subglacial geologic structures in the WIS grounding zone. We found that the water column within the ~500 km² embayment at the mouth of WIS is generally less than 50 m. This thin water column and its small gradient within the embayment indicate that the ocean water is likely well mixed, and sub-ice-shelf melting is slower than in a thicker, more stratified water column. This, in turn, suggests that the upstream end of the embayment is likely fed more by sediments subglacially transported from grounded ice than sediment melting out of the overriding ice. Melt-derived sediment is instead likely to be distributed over a long distance beneath the ice shelf. Holland [2008] concluded that the tidally well-mixed zone near the grounding line is generally small, and the customary view of the stratified ocean is adequate for most grounding zones. Applying his model insights to the geometry indicated by our results, however, shows that the well-mixed zone

likely extends tens of kilometers from the grounding line in our survey area.

[49] Based on the negative free-air gravity anomaly and its steep gradient near the grid-southern edge of the embayment, we modeled a sedimentary basin and a fault in the basement rock, consistent with results of previous gravity and seismic investigations in and around the Siple Coast. The current grounding line is located near or on a region of thin upper sediment with a basal topographic high. Because paleo-evidence indicates that the grounding line stabilized near its current location recently, the geologic setting there suggests that the site of stabilization may have been controlled in part by the underlying subglacial geology. Also, the fault we modeled aligns with the boundary of the CIR if linearly extended, which, together with previous seismic studies, may indicate a tectonic origin for CIR on a horst. We thus hypothesize that the subglacial geology may be playing an important role in the location and formation of the Siple Coast grounding zone.

[50] Our results come from data over a relatively limited area and should be subject to further testing with additional observations. Direct access to the water column by drilling through the ice shelf, planned for 2013–2014 Antarctic field season as part of WISSARD Program, will reveal the water properties and the tidal processes, as well as provide valuable data for ice-ocean modeling. Seismic-refraction surveys will further constrain the depth and the structures of the basement rock. Also, airborne gravity data, such as those of NASA's Operation IceBridge [Koenig et al., 2010] and ICECAP [Young et al., 2011], will enable us to extend the results of our ground-based gravity survey. Additionally, modeling of the sedimentary and basement structures along the flow of WIS over a more substantial distance (e.g., >100 km) may aid in revealing the history of grounding-line migration

and presence or absence of stabilization points. Conducting such surveys at other parts of the Siple Coast will provide a fuller understanding of the evolution of the ice streams and physical processes occurring there, and contribute to better projections of the future state of the WAIS.

[51] **Acknowledgments.** We thank Ken Jezek and Chris Jekeli of Ohio State University for the loan of the gravimeter, and Yves Rogister for providing the absolute gravity measurement at McMurdo Station. We also thank members of WISSARD 2011–12 field team (Lucas Beem, Rory Hart, Matthew Hill, Benjamin Peterson, and Matthew Siegfried) who assisted in data collection. Field logistics support was provided by Raytheon Polar Services Co. and New York Air National Guard. We thank the editor and two anonymous reviewers whose comments improved the text. This research was supported in part by NSF through 0424589, 0131487, 0838763, 0838764, and 0909335.

References

- Albert, D. G., and C. R. Bentley (1990), Seismic studies on the grid eastern half of the Ross Ice Shelf: RIGGS I and RIGGS II, in *The Ross Ice Shelf: Glaciology and Geophysics*, Antarct. Res. Ser., 42, edited by C. R. Bentley and D. E. Hayes, pp. 87–108, American Geophysical Union, Washington, D.C.
- Alley, R. B., D. D. Blankenship, C. R. Bentley, and S. T. Rooney (1987), Till beneath ice stream B: 3. Till deformation: Evidence and implications, *J. Geophys. Res.*, 92(B9), 8921–8929, doi:10.1029/JB092iB09p08921.
- Alley, R. B., D. D. Blankenship, S. T. Rooney, and C. R. Bentley (1989), Sedimentation beneath ice shelves - the view from Ice Stream B, *Mar. Geol.*, 85, 101–120, doi:10.1016/0025-3227(89)90150-3.
- Alley, R. B., S. Anandakrishnan, T. Dupont, B. R. Parizek, and D. Pollard (2007), Effect of Sedimentation on Ice-Sheet Grounding-Line Stability, *Science*, 315, 1838–1841, doi:10.1126/science.1138396.
- Anandakrishnan, S., D. D. Blankenship, R. B. Alley, and P. L. Stoffa (1998), Influence of subglacial geology on the position of a West Antarctic ice stream from seismic observations, *Nature*, 394, 62–65, doi:10.1038/27889.
- Anandakrishnan, S., G. A. Catania, R. B. Alley, and H. J. Horgan (2007), Discovery of Till Deposition at the Grounding Line of Whillans Ice Stream, *Science*, 315, 1835–1838, doi:10.1126/science.1138393.
- Behrendt, J. C., W. E. LeMasurier, A. K. Cooper, F. Tessensohn, A. Treuu, and D. Damaske (1991), Geophysical studies of the West Antarctic Rift system, *Tectonics*, 10, 1257–1273.
- Bell, R. E., M. Studinger, G. Karner, C. A. Finn, and D. D. Blankenship (2006), Identifying major sedimentary basins beneath the West Antarctic Ice Sheet from Aeromagnetic data analysis, in *Antarctica: Contributions to global earth sciences*, edited by D. K. Fütterer, D. Damaske, G. Kleinschmidt, H. Miller, and F. Tessensohn, pp. 117–122, Springer-Verlag, Berlin, Heidelberg, New York.
- Bentley, C. R. (1987), Antarctic ice streams: a review, *J. Geophys. Res.*, 92(B9), 8843–8858, doi:10.1029/JB092iB09p08843.
- Bindschadler, R. (1993), Siple Coast Project research of Cray Ice Rise and the mouths of Ice Stream B and C, West Antarctica: review and new perspectives, *J. Glaciol.*, 39(133), 538–552.
- Bindschadler, R. A., M. A. King, R. B. Alley, S. Anandakrishnan, and L. Padman (2003), Tidally controlled stick-slip discharge of a West Antarctic ice stream, *Science*, 301, 1087–1089, doi:10.1126/science.1087231.
- Bindschadler, R., H. Choi, and ASAID Collaborators (2011), *High-resolution Image-derived Grounding and Hydrostatic Lines for the Antarctic Ice Sheet*. National Snow and Ice Data Center, Boulder, Colorado, USA. doi:10.7265/N56T0JK2.
- Blankenship, D. D., C. R. Bentley, S. T. Rooney, and R. B. Alley (1987), Till beneath ice stream B: 1. Properties derived from seismic travel times, *J. Geophys. Res.*, 92(B9), 8903–8911, doi:10.1029/JB092iB09p08903.
- Blankenship, D. D., D. L. Morse, C. A. Finn, R. E. Bell, M. E. Peters, S. D. Kempf, S. M. Hodge, M. Studinger, J. C. Behrendt, and J. M. Brozena (2001), Geologic controls on the initiation of rapid basal motion for West Antarctic ice streams: A geophysical perspective including new airborne radar sounding and laser altimetry results, in *The West Antarctic Ice Sheet: Behavior and Environment*, Antarct. Res. Ser., 77, edited by R. B. Alley and R. A. Bindschadler, pp. 105–121, AGU, Washington, D.C., doi:10.1029/AR077p0105.
- Carter, S. P., and H. A. Fricker (2012), The supply of subglacial meltwater to the grounding line of the Siple Coast, West Antarctica, *Ann. Glaciol.*, 53(60), 267–280, doi:10.3189/2012AoG60A119.
- Catania, G., C. Hulbe, H. Conway, T. A. Scambos, and C. F. Raymond (2012), Variability in the mass flux of the Ross ice streams, West Antarctica, over the last millennium, *J. Glaciol.*, 58, 741–752.
- Christianson, K., R. W. Jacobel, H. J. Horgan, S. Anandakrishnan, and R. B. Alley (2012), Subglacial Lake Whillans –Ice-penetrating radar and GPS observations of a shallow active reservoir beneath a West Antarctic ice stream, *Earth Planet. Sci. Lett.*, 331–332(0), 237–245, doi:10.1016/j.epsl.2012.03.013.
- Christoffersen, P., S. Tulaczyk, and A. Behar (2009), Basal ice sequences in Antarctic ice stream: Exposure of past hydrologic conditions and a principal mode of sediment transfer, *J. Geophys. Res.*, 115, F03034, doi:10.1029/2009JF001430.
- Conway, H., B. L. Hall, G. H. Denton, A. M. Gades, and E. D. Waddington (1999), Past and future grounding-line retreat of the West Antarctic Ice Sheet, *Science*, 286, 280–283, doi:10.1126/science.286.5438.280.
- Cooper, A. K., F. J. Davey, and K. Hinz (1991), Crustal extension and origin of sedimentary basins beneath the Ross Sea and Ross Ice Shelf, Antarctica, in *Geological evolution of Antarctica*, edited by M. R. A. Thomson et al., pp. 285–291, Cambridge University Press, Cambridge, U.K.
- Diehl, T. M., J. W. Holt, D. D. Blankenship, D. A. Young, T. A. Jordan, and F. Ferraccioli (2008), First airborne gravity results over the Thwaites Glacier catchment, West Antarctica, *Geochem. Geophys. Geosyst.*, 9, Q04011, doi:10.1029/2007GC001878.
- Dowdeswell, J. A., and E. M. G. Fugelli (2012), The seismic architecture and geometry of grounding-zone wedges formed at the marine margins of past ice sheets, *GSA Bulletin*, 124(11–12), 1750–1761, doi:10.1130/B30628.1.
- Dowdeswell, J. A., D. Ottesen, J. Evans, C. O’Cofaigh, and J. B. Anderson (2008), Submarine glacial landforms and rates of ice-stream collapse, *Geology*, 36, 819–822, doi:10.1130/G24808A.1.
- Filina, I. Y., D. D. Blankenship, M. Thoma, V. V. Lukin, V. N. Masolov, and M. K. Sen (2008), New 3D bathymetry and sediment distribution in Lake Vostok: Implication for pre-glacial origin and numerical modeling of the internal processes within the lake, *Earth Planet. Sci. Lett.*, 276, 106–114, doi:10.1016/j.epsl.2008.09.012.
- Fretwell, P., and 59 others (2013), Bedmap2: improved ice bed, surface and thickness datasets for Antarctica, *The Cryosphere*, 7, 375–393, doi:10.5194/tc-7-375-2013.
- Fricker, H. A., et al. (2010), Siple Coast subglacial aquatic environments: The Whillans Ice Stream Subglacial Access Research Drilling (WISSARD) project, in *Subglacial Antarctic Aquatic Environments*, *Geophys. Monogr. Ser.*, vol. 192, edited by M. Siegert, C. Kennicutt, and B. Bindschadler, pp. 199–219, AGU, Washington, D.C.
- Greschar, L. L., C. R. Bentley, and L. R. Whiting (1992), An analysis of gravity measurements on the Ross Ice Shelf, Antarctica, in *Contributions to Antarctic Research III*, Antarctic Research series, edited by D. H. Elliot, 57, 105–155, American Geophysical Union, Washington, D.C.
- Hackney, R. L., and W. E. Featherstone (2003), Geodetic versus geophysical perspectives of the gravity anomaly, *Geophys. J. Int.*, 154, 35–43, doi:10.1046/j.1365-246X.2003.01941.x.
- Haran, T., J. Bohlander, T. Scambos, T. Painter, and M. Fahnestock (2006), MODIS mosaic of Antarctica (MOA) image map. National Snow and Ice Data Center, Boulder, CO. Digital media: <http://nsidc.org/data/moa/>.
- Holland, P. R. (2008), A model of tidally dominated ocean processes near ice shelf grounding lines, *J. Geophys. Res.*, 113, C11002, doi:10.1029/2007JC004576.
- Holland, D. M., S. S. Jacobs, and A. Jenkins (2003), Modelling the ocean circulation beneath the Ross Ice Shelf, *Antarct. Sci.*, 15(1), 13–23, doi:10.1017/S0954102003001019.
- Horgan, H. J., S. Anandakrishnan, R. W. Jacobel, K. Christianson, R. B. Alley, D. S. Heeszel, S. Picotti, and J. I. Walter (2012), Subglacial Lake Whillans –seismic observations of a shallow active reservoir beneath a West Antarctic ice stream, *Earth Planet. Sci. Lett.*, 331–332(0), 201–209, doi:10.1016/j.epsl.2012.02.023.
- Horgan, H. J., R. B. Alley, K. Christianson, R. W. Jacobel, S. Anandakrishnan, A. Muto, L. H. Beem, and M. R. Siegfried (2013), Estuaries beneath ice sheets, *Geology*, in press.
- Huerta, A. D., and D. L. Harry (2007), The transition from diffuse to focused extension: Modeled evolution of the West Antarctic Rift system, *Earth and Planet. Sci. Lett.*, 225, 133–147, doi:10.1016/j.epsl.2006.12.011.
- Hughes, T. (1977), West Antarctic ice streams, *Rev. Geophys.*, 15(1), 1–46, doi:10.1029/RG015i001p00001.
- Hulbe, C. L., and M. A. Fahnestock (2004), West Antarctic ice-stream discharge variability: mechanism, controls and pattern of grounding-line retreat, *J. Glaciol.*, 50(171), 471–484, doi:10.3189/172756504781829738.
- Jacoby, W., and P. L. Smilde (2009), *Gravity Interpretation: Fundamentals and Application of Gravity Inversion and Geologic Interpretation*, Springer, Berlin, Heidelberg.
- Jenkins, A., and C. S. M. Doake (1991), Ice-ocean interaction on Ronne Ice Shelf, Antarctica, *J. Geophys. Res.*, 96, 791–813, doi:10.1029/90JC01952.
- Joughin, I., and R. B. Alley (2011), Stability of the West Antarctic ice sheet in a warming world, *Nat. Geosci.*, 4, 506–513, doi:10.1038/ngeo1194.
- Kamb, B. (2001), Basal zone of the West Antarctic Ice Streams and its role in lubrication of their rapid motion, in *The West Antarctic Ice Sheet*

- Behavior and Environment*, Antarct. Res. Ser., 77, edited by R. B. Alley and R. A. Bindschadler, pp. 157–199, AGU, Washington, D.C., doi:10.1029/AR077p0157.
- Karner, G. D., M. Studinger, and R. E. Bell (2005), Gravity anomalies of sedimentary basins and their mechanical implications: Application to the Ross Sea basins, West Antarctica, *Earth Planet. Sci. Lett.*, 235, 577–596, doi:10.1016/j.epsl.2005.04.016.
- King, M. A., R. J. Bingham, P. Moore, P. L. Whitehouse, M. J. Bentley, and G. A. Milne (2012), Lower satellite-gravimetry estimates of Antarctic sea-level contribution, *Nature*, 491, 586–589, doi:10.1038/nature11621.
- Koenig, L., S. Martin, M. Studinger, and J. Sonntag (2010), Polar Airborne Observations Fill Gap in Satellite Data, *Eos. Trans. AGU*, 91(38), doi:10.1029/2010eo380002.
- Kohnen, H., and C. R. Bentley (1973), Seismic refraction and reflection measurements at “Byrd” Station, Antarctica, *J. Glaciol.*, 12(64), 101–111.
- Koth, K. R., and A. J. Long (2012), Microgravity methods for characterization of groundwater-storage changes and aquifer properties in the Karstic Madison Aquifer in the Black Hills of South Dakota, 2009–12, *U.S. Geological Survey Scientific Investigations Report 2012-5158*, 22 p.
- Lewis, E. L., and R. G. Perkin (1986), Ice pumps and their rates, *J. Geophys. Res.*, 91, 11,756–11,762, doi:10.1029/JC091iC10p11756.
- Li, Y., and D. W. Oldenburg (1998), 3-D inversion of gravity data, *Geophysics*, 63(1), 109–119.
- Longman, I. M. (1959), Formulas for computing the tidal accelerations due to the moon and sun, *J. Geophys. Res.*, 64, 2351–2355, doi:10.1029/JZ064i012p02351.
- Lowrie, W. (2007), *Fundamentals of geophysics*, Cambridge University Press, Cambridge, UK.
- Makinson, K., M. A. King, K. W. Nicholls, and G. H. Gudmundsson (2012), Diurnal and semidiurnal tide-induced lateral movement of Ronne Ice Shelf, Antarctica, *Geophys. Res. Lett.*, 39, L10501, doi:10.1029/2012GL051636.
- Mosola, A. B., and J. B. Anderson (2006), Expansion and rapid retreat of the West Antarctic Ice Sheet in eastern Ross Sea: possible consequence of over-extended ice streams?, *Quat. Sci. Rev.*, 25, 2177–2196, doi:10.1016/j.quascirev.2005.12.013.
- Munson, C. G., and C. R. Bentley (1992), The crustal structure beneath ice stream C and ridge BC, West Antarctica from seismic refraction and gravity measurements, in *REcent Progress in Antarctic Earth Science*, edited by Y. Yoshida, K. Kamimura, and K. Shiraishi, pp. 507–514, TERRAPUB, Tokyo.
- Muto, A., S. Anandakrishnan, and R. B. Alley (2013), Subglacial bathymetry and sediment layer distribution beneath the Pine Island Glacier ice shelf modeled using aerogravity and autonomous underwater vehicle data, *Ann. Glaciol.*, 56(64), 27–32, doi:10.3189/2013AoG64A110.
- Nafe, J. E., and C. L. Drake (1963), Physical properties of marine sediments, in *The Sea*, 3, edited by M. N. Hill, pp. 794–815, Interscience, New York.
- Oldenburg, D. W. (1974), The inversion and interpretation of gravity anomalies, *Geophysics*, 39(4), 526–536.
- Onizawa, S., H. Mikada, H. Watanabe, and S. Sakashita (2002), A method for simultaneous velocity and density inversion and its application to exploration of subsurface structure beneath Izu-Oshima volcano, Japan, *Earth Planets Space*, 54, 803–817.
- Padman, L., S. Erofeeva, and I. Joughin (2003), Tides of the Ross Sea and Ross Ice Shelf cavity, *Antarctic Science*, 15(1), 31–40, doi:10.1017/S0954102003001032.
- Parker, R. L. (1973), The rapid calculation of potential anomalies, *Geophys. J. Roy. Astron. Soc.*, 31, 447–455.
- Peters, L. E., S. Anandakrishnan, R. B. Alley, and A. M. Smith (2007), Extensive storage of basal meltwater in the onset region of a major West Antarctic ice stream, *Geology*, 35(3), 251–254, doi:10.1130/G23222A.1.
- Plouff, D. (1976), Gravity and magnetic fields of polygonal prisms and application to magnetic terrain corrections, *Geophysics*, 41, 727–741.
- Rignot, E., J. Mouginot, and B. Scheuchl (2011a), Ice Flow of the Antarctic Ice Sheet, *Science*, 333, 1427–1430, doi:10.1126/science.1208336.
- Rignot, E., J. Mouginot, and B. Scheuchl (2011b), Antarctic Grounding Line Mapping from Differential Satellite Radar Interferometry, *Geophys. Res. Lett.*, 38, L10504, doi:10.1029/2011GL047109.
- Robertson, J. D., and C. R. Bentley (1990), Seismic studies on the grid western half of the Ross Ice Shelf: RIGGS I and RIGGS II, in *The Ross Ice Shelf: Glaciology and Geophysics*, Antarct. Res. Ser., 42, edited by C. R. Bentley and D. E. Hayes, pp. 55–86, American Geophysical Union, Washington D.C.
- Robertson, J. D., C. R. Bentley, J. W. Clough, and L. L. Gerischar (1982), Sea bottom topography and crustal structure below the Ross Ice Shelf, Antarctica, in *Antarctic Geoscience*, edited by C. Craddock, pp. 1083–1090, Univ. of Wisconsin Press, Madison, WI.
- Rooney, S. T., D. D. Blankenship, and C. R. Bentley (1987), Seismic refraction measurements of crustal structure in West Antarctica, in *Gondwana Six: Structure, Tectonics, and Geophysics*, Geophysical Monograph Series, 40, edited by G. D. McKenzie, pp. 1–7, American Geophysical Union, Washington D.C.
- Rooney, S. T., D. D. Blankenship, R. B. Alley, and C. R. Bentley (1991), Seismic reflection profiling of a sediment-filled graben beneath ice stream B, West Antarctica, in *Geological Evolution of Antarctica*, edited by M. R. A. Thomson, J. A. Crame, and J. W. Thomson, pp. 261–265, Cambridge University Press, Cambridge, U.K.
- Roy, L., M. K. Sen, D. D. Blankenship, P. L. Stoffa, and T. G. Richter (2005), Inversion and uncertainty estimation of gravity data using simulated annealing: an application over Lake Vostok, East Antarctica, *Geophysics*, 70(1), J1–J12, doi:10.1190/1.1852777.
- Sandwell, D. T. (1987), Biharmonic Spline Interpolation of GEOS-3 and SEASAT Altimeter Data, *Geophys. Res. Lett.*, 14(2), 139–142, doi:10.1029/GL014i002p00139.
- Schoof, C. (2007), Ice sheet grounding line dynamics: steady states, stability, and hysteresis, *J. Geophys. Res.*, 112, F03S28, doi:10.1029/2006JF000664.
- Scintrex Limited (2012), CG-5 Operation Manual Revision 8, Ontario, Canada, downloaded from <http://scintrexlt.com> on January, 2013.
- Severinghaus, J. P., et al. (2010), Deep air convection in the firm at a zero-accumulation site, central Antarctica, *Earth Planet. Sci. Lett.*, 293, 359–367, doi:10.1016/j.epsl.2010.03.003.
- Shepherd, A. 46 others (2012), A Reconciled Estimate of Ice-Sheet Mass Balance, *Science*, 338, 1183–1189, doi:10.1126/science.1228102.
- Studinger, M., R. E. Bell, and A. A. Tikku (2004), Estimating the depth and shape of subglacial Lake Vostok’s water cavity from aerogravity data, *Geophys. Res. Lett.*, 31, L12401, doi:10.1029/2004GL019801.
- Tinto, K. J., and R. E. Bell (2011), Progressive unpinning of Thwaites Glacier from newly identified offshore ridge: Constraints from aerogravity, *Geophys. Res. Lett.*, 38, L20503, doi:10.1029/2011GL049026.
- Todd, C., J. Stone, H. Conway, B. Hall, and G. Bromley (2010), Late Quaternary evolution of Reedy Glacier, Antarctica, *Quat. Sci. Rev.*, 29(11–12), 1328–1341, doi:10.1016/j.quascirev.2010.02.001.
- Torge, W. (1989), *Gravimetry*, Walter de Gruyter, Berlin, New York, NY.
- Turcotte, D. L., and G. Schubert (2002), *Geodynamics*, 2nd ed., Cambridge University Press, Cambridge, U.K.
- Van Wijk, J. W., J. F. Lawrence, and N. W. Driscoll (2008), Formation of the Transantarctic Mountains related to extension of the West Antarctic Rift system, *Tectonophysics*, 458, 117–126.
- Walker, R. T., K. Christianson, B. R. Parizek, S. Anandakrishnan, and R. B. Alley (2012), A viscoelastic flowline model applied to tidal forcing of Bindschadler Ice Stream, West Antarctica, *Earth Planet. Sci. Lett.*, 319–320, 128–132, doi:10.1016/j.epsl.2011.12.019.
- Wessel, P., and A. B. Watts (1988), On the accuracy of marine gravity measurements, *J. Geophys. Res.*, 93(B1), 393–413, doi:10.1029/JB093iB01p00393.
- Williams, M. J. M., A. Jenkins, and J. Determann (1998), Physical controls on ocean circulation beneath ice shelves revealed by numerical models, in *Ocean, Ice, and Atmosphere: Interactions at the Antarctic Continental Margin*, Antarct. Res. Ser., 75, edited by S. S. Jacobs and R. F. Weiss, pp. 285–299, AGU, Washington, D.C., doi:10.1029/AR075p0285.
- Wilson, G. S., and K. J. Tinto (2009), Calibration values for gravity base stations, McMurdo Station and Scott Base, Ross Island, Antarctica, *Antarct. Sci.*, 21(4), 367–372, doi:10.1017/S0954102009001977.
- Young, D. A., et al. (2011), A dynamic early East Antarctic Ice Sheet suggested by ice covered fjord landscapes, *Nature*, 474, 72–75, doi:10.1038/nature10114.